applied optics

Dynamic compensation of gradient index rod lens aberrations by using liquid crystals

Louis Begel[1] and Tigran Galstian[1,2,*]

[1]Center for Optics, Photonics and Lasers, Department of Physics, Engineering Physics and Optics, Université Laval, 2375 Rue de la Terrasse, Québec, Québec G1V 0A6, Canada
[2]Lensvector Inc. and TLCL Optical Research Inc., 6203 San Ignacio Ave. Suite 110, San Jose, California 95119, USA
*Corresponding author: galstian@phy.ulaval.ca

Received 24 July 2018; revised 7 August 2018; accepted 9 August 2018; posted 13 August 2018 (Doc. ID 340576); published 10 September 2018

An electrically variable liquid crystal lens is used to compensate the aberrations of commercial gradient index rod lenses used for deep brain endoscopy. This is achieved by the use of a weakly conductive layer in the so-called "modal control" lens approach with a segmented peripheral electrode. The root mean square aberrations of the system are reduced by a factor of 4.3. The proposed solution can be used in many photonic applications using fixed optical components with high aberrations that have significant sample-to-sample variability.

https://doi.org/10.1364/AO.57.007618

1. INTRODUCTION

Several research and development groups are intensively working for the creation of high-quality optical endoscopic probes (so-called "miniscopes") that are used in brain imaging (see, e.g., Refs. [1–3]). Fixed-focus rod gradient index (R-GRIN) lenses must be used in those studies (see Fig. 1) to reach deep brain zones of interest (at several millimeters) given the strong scattering and absorption of light by the brain tissue at excitation and fluorescence wavelengths (e.g., at ≈488 nm and ≈514 nm for Alexa488, respectively [3]). Unfortunately, given the very small focal distance and depth of field of those systems, their surgical implantation is an extremely delicate task. Very frequently, the zone of interest (Fig. 1) may be missed during the implantation, which would result in the sacrifice of the animal.

In addition, many commercially available R-GRIN lenses have severe aberrations that change from sample to sample. While the simple defocus of those R-GRIN lenses may be easily compensated by adding a commercially available small lens of corresponding optical power (OP), their complex aberrations cannot be improved, unless costly deformable mirrors [4,5] or spatial light modulators (SLMs) [6] are used. However, those devices are large and cannot fit into implants (or probes) for freely behaving small animals (typically mice). At the same time, the need in adaptive optical components (to improve the quality of GRIN lens systems [5,7]) is omnipresent.

Recently, several research groups have proposed the use of miniature electrically tunable liquid crystal (LC) lenses (TLCLs) to improve the imaging quality (see, e.g., Refs. [8–10]). Many of them, including the one described by our group for endoscopic application [3], use a TLCL that is based on the principle of flat electrically variable GRIN lenses. Thus, it can address the first above-mentioned problem of focus tuning. However, by its design (using a single hole patterned electrode) (HPE) (see Fig. 2), this lens cannot change significantly the wavefront shape (to address the second issue).

Recently, we have introduced a TLCL with segmented electrodes to compensate the wavefront asymmetry of the lens [11]. In the present work, we report the use of the same TLCL to compensate the aberrations of a commercially available R-GRIN lens.

2. COMPENSATION OF GRIN LENS ABERRATIONS

Among various possible architectures used to build TLCLs (see, e.g., Refs. [8–10,12]), we have chosen the so-called "modal control" lenses [13,14] (Fig. 2), since they provide good OP variability range while keeping the optical quality very high (by the choice of the frequency and voltage of the excitation electrical signal [15]) as well as by keeping its electrical power consumption at very low levels (≈10 μW, [16]). Within this approach [Fig. 2(a)], an LC layer (in our case, a homemade mixture of thickness $L \approx 60$ μm, optical birefringence $\Delta n \approx 0.219$ and dielectric anisotropy $\varepsilon_a \approx 9$) is sandwiched between an HPE (defining the clear aperture (CA) of the lens; here CA ≈ 0.55 mm) and a uniform transparent electrode (typically made of indium tin oxide, ITO). A thin weakly conductive layer (WCL), typically with a sheet resistance $R_s \approx 40$ MOhm/sq), is cast over the HPE (in our case, ≈100 nm thick TiO layer) to soften the profile of the electric field along the x axis when the aspect ratio of the lens is large [17]:

$$\mathrm{CA}/L \gg 2.5. \tag{1}$$

The electric field inside of the LC layer [Fig. 2(a)] being stronger in the periphery ($x = \pm CA/2$) of such a structure (compared to its center at $x = 0$), the corresponding reorientation (from its ground state, parallel to cell substrates) of the local average alignment direction of LC molecules (the so-called director [18]) is stronger in those areas. This, in turn, reduces the local effective refractive index of the LC layer in the peripheral zones, thus generating an electrically variable GRIN lens.

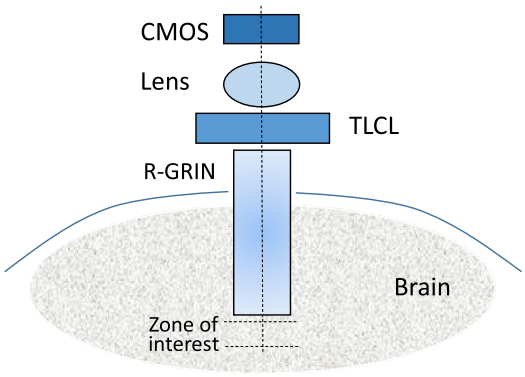

Fig. 1. Schematic demonstration of the miniscope and of its use to image deep brain zones of interest. CMOS, image sensor; TLCL, tunable liquid crystal lens; R-GRIN, rod gradient index lens.

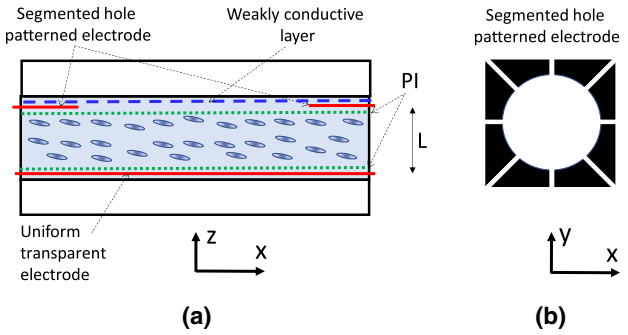

Fig. 2. Schematic demonstration of the TLCL using a segmented HPE and a uniform transparent electrode. (a) Side cross-section view of the modal control lens; ellipses show the local average molecular orientation direction; L, thickness of the LC layer; PI, alignment layers (dotted lines); dashed line represents the WCL; (b) schematic illustration (top view) of the HPE that is segmented into eight zones.

As we shall show hereafter, the segmentation of the peripheral electrode [Fig. 2(b)] into eight segments (we could name this lens as S-TLCL) can be used both for focus tuning as well as for the compensation of various aberrations of the R-GRIN. To demonstrate its capabilities, we have combined our S-TLCL (with eight segmented electrodes) with a commercial R-GRIN (from GOfoton, diameter $= 0.5 \pm 0.05$ mm, length $= 61.2$ mm, 2 pitch, NA ≈ 0.084), by simply attaching it to our element (this is the configuration that our miniscope uses, [3]) (Fig. 3). An unpolarized CW laser (operating at 543 nm) was used along with a beam expander (lens 1 and lens 2) to generate a normally incident Gaussian-shaped beam (transversal intensity distribution). A polarizer was used to align the polarization of the incident light to be parallel with the ground state orientation direction of the director of the S-TLCL. We have also used a relay lens (lens 3) to keep the image of the exit plane of the R-GRIN lens on the entrance plane of the Shack–Hartmann wavefront sensor (Fig. 3).

We start our experiments by the study of the case when the lens is driven with a single HPE (in fact, the same electric signal is applied to all eight segments). The control is performed by fixing the voltage value $U = 4$ V_{RMS} (root mean square, RMS) and by changing the frequency of the electrical signal from 0.5 to 4.0 kHz [19]. It may be worth noticing that we have also tested the cases of 3 V_{RMS} and 5 V_{RMS} and we found that, for the reference case (single segment HPE), the optimal value was the 4 V_{RMS}. Thus, in this case, as we can see from Fig. 4 (filled

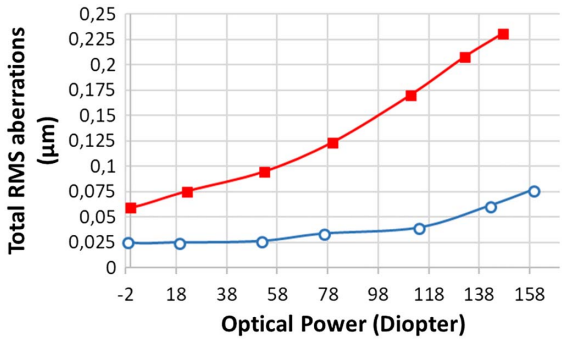

Fig. 4. Total RMS aberrations versus the OP of the system in the case of a single HPE (filled squares) and segmented HPE (open circles). The lens has a slight bend, causing a negative OP in the ground state. The corresponding voltage/frequency values are presented in Table 1.

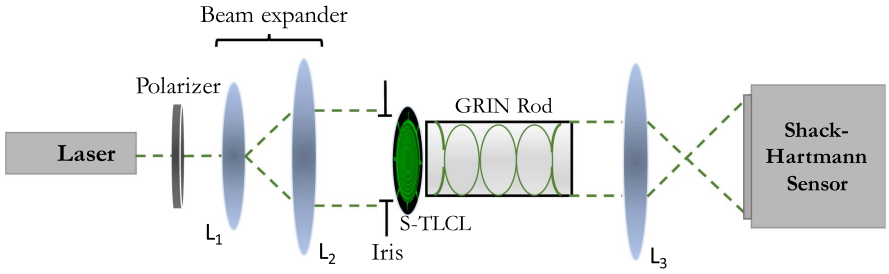

Fig. 3. Schematic demonstration of the experimental setup used to study the compensation of R-GRIN aberrations by using the modal control lens with segmented peripheral electrode. L1, 2, 3 are lenses.

Table 1. Voltages and Frequencies Applied to Eight Segments of the HPE

Frequency (kHz)	Segm.1 (V_{RMS})	Segm.2 (V_{RMS})	Segm.3 (V_{RMS})	Segm.4 (V_{RMS})	Segm.5 (V_{RMS})	Segm.6 (V_{RMS})	Segm.7 (V_{RMS})	Segm.8 (V_{RMS})
0.5	4		5	4			5	4
1	3.5	3	3.7	4		4.5	5.2	3.5
1.5	3.7		4.2	4.4	4.3		4.8	3.8
2	3.4	3.6	3.9	4.8	4.5	4.3	4.6	3.7
2.5	2.9	3.2	3.4	4.7	4.5	4	4.2	3.1
3	3	3.5	3.8	5.8	5.6	4.5	4.8	3.2
3.5	2.7	3.1	3.4	6.3	6.1	4.9	5.2	2.9
4	2.8	2.6	3.3	7.3	7	5.8	6.8	2.8

squares) the total RMS aberrations of the TLCL and R-GRIN increase noticeably along the increase of the OP of the TLCL. However, if we use different electrical signals (Table 1), applied to different segments of the HPE, we can then significantly (by a factor of 8) reduce those aberrations (Fig. 4, open circles). The corresponding values of voltages and frequencies (of Table 1) were obtained by an iterative optimization approach to minimize the total RMS aberrations.

The details of original aberrations of the R-GRIN (the aberrations of the TLCL in the OFF state are negligible) as well as of the compensated (by the activation of the S-TLCL) aberrations may be seen in Fig. 5. As we can see, the absolute values of the majority of Zernike coefficients are significantly reduced. Here is the summary of most important changes: astigmatism −45°/45° (Z4), from −0.039 to −0.005; astigmatism 0°/90° (Z6), from 0.032 to −0.004; coma X (Z8), from −0.035 to 0.0005; coma Y (Z9), from −0.029 to −0.0035 μm; trefoil Y (Z10), from −0.019 to −0.007 μm; spherical aberration (Z13), from 0.039 to −0.018 μm; and Z14, from −0.001 to 0.0165 μm. It is important to mention here that we have used the Shack–Hartmann wavefront sensor from Thorlabs (with a digital aperture of 500 μm), which automatically places the index 1 on the piston aberrations (under the index 0), which is shifting all coefficients with respect to the standard definition of Zernike coefficients.

Overall, the total RMS aberrations are reduced by a factor of ≈4.3 at 3 kHz, which is a rather significant improvement. Another important change, kept aside from this calculation, is the defocus (the change of Z5 resulting in the increase of the total OP of the system), which (as mentioned above) can be easily compensated by adding a small commercial lens, or a second TLCL that can provide adjustable negative OP (see, e.g., Refs. [8,20]).

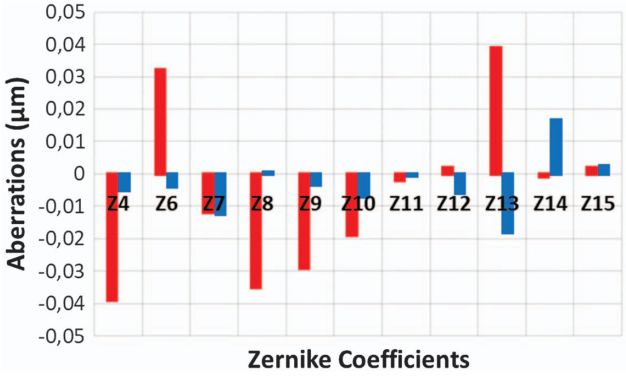

Fig. 5. Quantitative demonstration of wavefront errors' correction of an R-GRIN lens by using the developed S-TLCL; the red color corresponds to the original state, while the blue color corresponds to the corrected (by the S-TLCL) state.

Finally, we have to emphasize that the change of the OP and of the total RMS aberrations of the system is a continuous process (not a discrete switch), and it can be further optimized (Fig. 5 is just an example of possible improvements). When we need to change the OP's value of the system, we must readjust the voltages and frequencies applied to different segments to optimize the RMS aberrations again. Fortunately, once this is established, the process is reproducible.

To demonstrate the impact of the reduction (we have obtained here) on the image quality, we have performed an additional experiment by measuring the point spread function of our system. Before our correction, the resolution of the system (R-GRIN + TLCL) in x and y directions was, respectively, $r_x = 1.80$ μm and $r_y = 1.90$ μm, while after the correction, we obtain $r_x = 1.55$ μm and $r_y = 1.25$ μm. Thus, the average improvement of resolution is ≈32%, which is rather noticeable (see also Ref. [5] for similar improvements of RMS aberrations).

3. DISCUSSIONS AND CONCLUSIONS

We have demonstrated experimentally that the use of a WCL and the segmentation of the HPE (to obtain an S-TLCL within the modal control design) may be used to obtain advanced wavefront control capability. Compared to the single HPE case, the cost of the lens manufacturing is the same (single lithographic process), while its capacities are significantly enhanced. It is worth mentioning that the cost of connecting eight electrodes (instead of one), the corresponding electrical driver and control complexity may be higher; however, the LCD industry is used to handle such situations (with thousands of connectors). The short-term potential of this approach is demonstrated by focus tuning or compensating (reducing by a factor of 4.3) the aberrations of a commercial R-GRIN lens that was combined with the S-TLCL [21]. An improvement of resolution is also demonstrated. We think that, given the importance of those aberrations, and, in addition, their significant sample-to-sample variations, the proposed S-TLCL may find applications is many other optical systems and enable new design possibilities.

Acknowledgment. This research was supported by the Canada Research Chair in Liquid Crystals and Behavioral Biophotonics held by T. Galstian, who also has received the Manning Innovation Award in 2014. We would like also to thank the R&D team of LensVector for providing the WCL, their homemade LC mixture and supporting us with their advice.

REFERENCES

1. K. K. Ghosh, L. D. Burns, E. D. Cocker, A. Nimmerjahn, Y. Ziv, A. El Gamal, and M. J. Schnitzer, "Miniaturized integration of a fluorescence microscope," Nat. Methods **8**, 871–878 (2011).
2. http://miniscope.org/index.php/Main_Page.
3. A. Bagramyan, T. Galstian, and A. Saghatelyan, "Motion-free endoscopic system for brain imaging at variable focal depth using liquid crystal lenses," J. Biophoton. **10**, 762–774 (2017).
4. E. Dalimier and C. Dainty, "Comparative analysis of deformable mirrors for ocular adaptive optics," Opt. Express **13**, 4275–4285 (2005).
5. W. Lee and S. Yun, "Adaptive aberration correction of GRIN lenses for confocal endomicroscopy," Opt. Lett. **36**, 4608–4610 (2011).
6. G. D. Love, "Wave-front correction and production of Zernike modes with a liquid-crystal spatial light modulator," Appl. Opt. **36**, 1517–1524 (1997).
7. C. Wang and N. Ji, "Characterization and improvement of three-dimensional imaging performance of GRIN-lens-based two-photon fluorescence endomicroscopes with adaptive optics," Opt. Express **21**, 27142–27154 (2013).
8. T. V. Galstian, *Smart Mini-Cameras* (CRC Press, 2013).
9. G. Li, "Adaptive lens," Prog. Opt. **55**, 199–283 (2010).
10. Y.-H. Lin, Y.-J. Wang, and V. Reshetnyak, "Liquid crystal lenses with tunable focal length," Liq. Cryst. Rev. **5**, 111–143 (2017).
11. L. Begel and T. Galstian, "Liquid crystal lens with corrected wavefront asymmetry," Appl. Opt. **57**, 5072–5078 (2018).
12. S. Sato, "Applications of liquid crystals to variable-focusing lenses," Opt. Rev. **6**, 471–485 (1999).
13. A. Naumov, M. Y. Loktev, I. R. Guralnik, and G. Vdovin, "Liquid-crystal adaptive lenses with modal control," Opt. Lett. **23**, 992–994 (1998).
14. A. Naumov, G. D. Love, M. Y. Loktev, and F. L. Vladimirov, "Control optimization of spherical modal liquid crystal lenses," Opt. Express **4**, 344–352 (1999).
15. T. Galstian, K. Asatryan, V. Presniakov, A. Zohrabyan, A. Tork, A. Bagramyan, S. Careau, M. Thiboutot, and M. Cotovanu, "High optical quality electrically variable liquid crystal lens using an additional floating electrode," Opt. Lett. **41**, 3265–3268 (2016).
16. T. Galstian, O. Sova, K. Asatryan, V. Presniakov, A. Zohrabyan, and M. Evensen, "Optical camera with liquid crystal autofocus lens," Opt. Express **25**, 29945–29964 (2017).
17. S. Yanase, K. Ouchi, and S. Sato, "Molecular orientation analysis of a design concept for optical properties of liquid crystal microlenses," Jpn. J. Appl. Phys. **40**, 6514–6521 (2001).
18. P.-G. de Gennes and J. Prost, *The Physics of Liquid Crystals*, Vol. **83** of International Series of Monographs on Physics (Clarendon Press, 1995).
19. A. Zohrabyan, T. Galstian, K. Asatryan, V. Presniakov, M. Thiboutot, A. Bagramyan, A. Tork, J. J. Parker, T. Cooper, and B. Khodadad, "In-flight auto focus method and system for tunable liquid crystal optical element," U.S. patent 15,196,421 (29 June 2016).
20. B. Wang, M. Ye, and S. Sato, "Liquid crystal lens with focal length variable from negative to positive values," IEEE Photon. Technol. Lett. **18**, 79–81 (2006).
21. T. Galstian, A. Saghatelyan, and A. Bagramyan, "Tunable optical device, tunable liquid crystal lens assembly and imaging system using same," U.S. patent 12,542,458 (26 May 2016).